Journal of Zhejiang University-SCIENCE A (Applied Physics & Engineering)
ISSN 1673-565X (Print); ISSN 1862-1775 (Online)
www.zju.edu.cn/jzus; www.springerlink.com
E-mail: jzus@zju.edu.cn

Predictive control of a direct internal reforming SOFC using a self recurrent wavelet network model*

Jun LI[†1], Nan GAO[2], Guang-yi CAO[1], Heng-yong TU[1], Ming-ruo HU[1], Xin-jian ZHU[1], Jian LI[3]

([1]*Institute of Fuel Cell, Department of Automation, Shanghai Jiao Tong University, Shanghai 200240, China*)

([2]*Department of Mathematics, Shanghai University, Shanghai 200444, China*)

([3]*College of Materials Science and Engineering, Huazhong University of Science and Technology, Wuhan 430074, China*)

[†]E-mail: jun.li.fc@gmail.com

Received Dec. 31, 2008; Revision accepted Mar. 12, 2009; Crosschecked Oct. 18, 2009

Abstract: In this paper, an application of a nonlinear predictive controller based on a self recurrent wavelet network (SRWN) model for a direct internal reforming solid oxide fuel cell (DIR-SOFC) is presented. As operating temperature and fuel utilization are two important parameters, the SOFC is identified using an SRWN with inlet fuel flow rate, inlet air flow rate and current as inputs, and temperature and fuel utilization as outputs. To improve the operating performance of the DIR-SOFC and guarantee proper operating conditions, the nonlinear predictive control is implemented using the off-line trained and on-line modified SRWN model, to manipulate the inlet flow rates to keep the temperature and the fuel utilization at desired levels. Simulation results show satisfactory predictive accuracy of the SRWN model, and demonstrate the excellence of the SRWN-based predictive controller for the DIR-SOFC.

Key words: Direct internal reforming (DIR), Solid oxide fuel cell (SOFC), Predictive control, Self recurrent wavelet network (SRWN)

doi:10.1631/jzus.A0800887 **Document code:** A **CLC number:** TP273; TM911.4

1 Introduction

As a highly efficient and environmentally friendly source of electrical energy, the solid oxide fuel cell (SOFC) has become one of the most attractive technologies for power generation during recent decades. This type of fuel cell functions at relatively high temperature (up to 1000 °C) with air as the oxidant and hydrogen (also carbon monoxide) as the fuel. Moreover, the operating temperature is high enough to allow for internal reforming to produce hydrogen from hydrocarbons within the stack itself (Larminie and Dicks, 2000).

A direct internal reforming SOFC (DIR-SOFC) should operate under suitable conditions, such that optimum performance can be obtained and the lifetime of the device can be effectively extended. Extreme operating conditions (e.g., too low fuel utilization, too high or low temperature) will lead to low efficiency and high pollution and even to permanent damage to the SOFC. Operating parameters are coupled variously to each other, changing their influence on the SOFC, leading to increased complexity in the relationship between inputs and outputs. Therefore, the SOFC is viewed as a nonlinear multi-input and multi-output (MIMO) system, and the control of the SOFC becomes an important issue.

A key part of the controller design is the modeling of the process. In recent years, many models (Karoliussen *et al.*, 1998; Campanari, 2001; Chan *et al.*, 2003; Stiller *et al.*, 2005) have been proposed to study the performance of SOFCs. Karoliussen *et al.* (1998) developed a mathematical model of a cross-

* Project supported by the National High-Tech Research and Development Program (863) of China (No. 2006AA05Z148), and the Shanghai Municipal Natural Science Foundation, China (No. 08ZR1409800)

flow planar SOFC stack. The coupled partial differential equations (PDEs) in the model were transformed into finite difference equations to implement the numerical simulation. Campanari (2001) presented a thermodynamic model of a tubular SOFC stack with internal air preheating and internal fuel reforming. Thermodynamic and parametric analyses of the SOFC stack were carried out and discussed. Stiller *et al.* (2005) constructed two 2D steady-state models for tubular and planar SOFCs. Based on these models, two SOFC-GT (gas turbine) hybrid systems were developed and their operating performance and parameter influences were studied. Most of these models, which were derived from principles of chemical reaction kinetics, heat transfer and mass conservation, can well describe the various physical and chemical phenomena within SOFCs. However, their complexity and long computational time make it difficult to apply these models to real-time control systems.

In the recent literature (Arriagada *et al.*, 2002; Shen *et al.*, 2002; Jurado, 2006a; 2006b; Entchev and Yang, 2007), some black-box approaches based on measurements without any physical or chemical explanation were used for modeling fuel cells. Arriagada *et al.* (2002) developed an SOFC model based on an artificial neural network (ANN) to simulate a planar SOFC. Jurado (2006a) employed the Hammerstein system to model the SOFC for static and dynamic performance studies. Jurado (2006b) used a fuzzy block to represent the nonlinear subsystem in the Hammerstein system. Entchev and Yang (2007) used ANN and adaptive neuro-fuzzy inference system (ANFIS) techniques to identify a residential SOFC system to predict SOFC performance parameters.

The traditional ANN is constructed using multi-layer perceptron based on the back propagation (BP) or gradient descent training method. It is difficult to guarantee a good performance for controlling real-time industrial processes using an ANN-based predictive controller owing to the multi-layer structure and slow convergence resulting from use of the gradient descent method. Among the data-driven methods, the wavelet networks (WNs) combine the capability of wavelet reconstruction and the capability of neural networks in learning from processes (Zhang and Benveniste, 1992). It has been proven that WNs with a finite number of wavelets can approximate a wide range of nonlinear functions to any desired degree of accuracy (Chui, 1992). The advantages of the wavelet multi-resolution approximation (MRA) and ANN-like structure guarantee the good convergence of the WN. Because of the finite support and self-similarity properties of a WN, it can be used for approximating unknown nonlinear functions with local nonlinearities and fast variations. However, without the aid of tapped delay units, an ANN or WN using feedforward network structure cannot describe a dynamic relationship between inputs and outputs, and thus is unsuitable for solving temporal problems. Hence, feedback and recurrent WNs are applied to the identification and control of nonlinear dynamic systems (Oussar *et al.*, 1998; Lin *et al.*, 2002; Lin and Wang, 2006; Yoo *et al.*, 2006), which benefit from attractor dynamics and signal storage for later use. The self recurrent WN (SRWN) is obtained by modifying the original WN, and has a wavelet layer composed of internal feedback nodes. This feature allows the past information of the network to be retained for a certain period of time, and improves the capability of the WN for representing the nonlinear dynamic behavior of the process. Hence, the SRWNs combine the properties of the fast convergence of WNs with the attractor dynamics of recurrent networks (Yoo *et al.*, 2006). The simulated and experimental results obtained by control systems based on WN and SRWN show good robust performances in response to external disturbances and uncertainties (Lin *et al.*, 2002; Yoo *et al.*, 2006).

In this paper, we use the SRWN to identify a DIR-SOFC and employ the resulting SRWN model (off-line and on-line training) as the predictive model in the predictive control structure. The inlet fuel flow rate and the inlet air flow rate are regulated to keep the operating temperature and fuel utilization at the set points when the load current changes.

2 DIR-SOFC plant description

The configuration of the whole SOFC plant with direct internal reforming is illustrated in Fig. 1. Methane is used as fuel and is mixed with a part of the anode flue gas after compression. Preheated by the exhaust gas in heat exchangers, the steam-methane gas mixture and the air are injected separately into the

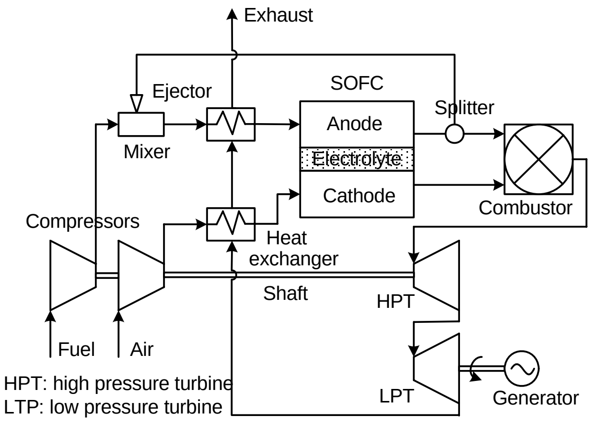

Fig. 1 Schematic diagram of a direct internal reforming solid oxide fuel cell (DIR-SOFC) plant

anode and the cathode. At the anode, the methane is reformed into hydrogen and carbon monoxide which are consumed in the electrochemical reactions to generate electric power. The heat required for endothermic reforming reactions is supplied by concurrent exothermic electrochemical reactions (Chan *et al.*, 2003). Reactions occurring in the SOFC are as follows:

Reforming reactions:

$$CH_4 + 2H_2O \leftrightarrow CO_2 + 4H_2, \tag{1}$$

$$CH_4 + H_2O \leftrightarrow CO + 3H_2. \tag{2}$$

Water-gas shift reaction:

$$CO + H_2O \leftrightarrow CO_2 + H_2. \tag{3}$$

Electrochemical reactions:

Anode:

$$H_2 + O^{2-} \rightarrow H_2O + 2e^-, \tag{4}$$

$$CO + O^{2-} \rightarrow CO_2 + 2e^-; \tag{5}$$

Cathode:

$$\frac{1}{2}O_2 + 2e^- \rightarrow O^{2-}. \tag{6}$$

The remaining part of the cathode and anode flue gases is supplied to a combustor to burn the unused fuel. The combusted gas mixture is expanded in a high pressure turbine (HPT) with variable shaft speed driving the compressors. In a low pressure turbine (LPT), the flue gas is expanded to atmospheric pressure (Stiller *et al.*, 2005), which drives the synchronous generator to produce AC electric power. Typically 60%~70% of the total power is the DC power produced by the SOFC stack (Selimovic and Palsson, 2002). Although the AC power supplied by the generator is a small part of the total power, it greatly increases the overall electrical efficiency of the system.

3 SRWN model

The SRWN illustrated in Fig. 2 is composed of four layers: an input layer, a mother wavelet layer, a multi-dimensional wavelet layer and an output layer. In layer 2, each node consists of a scaled and translated wavelet ψ_{li} and a delayed self-feedback loop, which stores the past information of the node. Furthermore, to construct multi-dimensional wavelets for a multi-input system, each node in layer 3 is denoted by Π, which multiplies the input signals and outputs the result of the product, i.e., the product of mono-dimensional wavelets with respect to the input node. The single node in the output layer is labeled as Σ, which calculates the overall output as the summation of all input signals. In this study, the first derivative of a Gaussian function $\psi(x)=-x\exp(-x^2/2)$ is adopted as a mother wavelet. The input-output relation of the SRWN is expressed as

$$f = \sum_{l=1}^{N_\mathrm{w}} w_l \prod_{i=1}^{N_\mathrm{in}} \psi\left(\frac{x_i + \beta_{li}\psi_{li}(k-1) - b_{li}}{a_{li}}\right) + \sum_{i=1}^{N_\mathrm{in}} \alpha_i x_i\,, \tag{7}$$

where N_w is the total number of the nodes in layer 3, N_in is the number of inputs, and β_{li} is the weight of the past output signal of ψ_{li}. The connecting weight w_l is the output action strength associated with the lth multi-dimensional wavelet in layer 3, and a_{li} and b_{li} are the dilation and translation parameters of the lith wavelet in layer 2, respectively. The second term on the right side of Eq. (7), described by the summation of weighted inputs, represents the linear part of the plant.

The objective function is chosen as follows:

$$J(k) = \frac{1}{2}\sum_{j=1}^{k}\left(y(j) - \hat{y}(j)\right)^2 \lambda^{k-j}, \tag{8}$$

where $\hat{y}(j)$ is the SRWN output value related to example j, and λ is the forgetting factor.

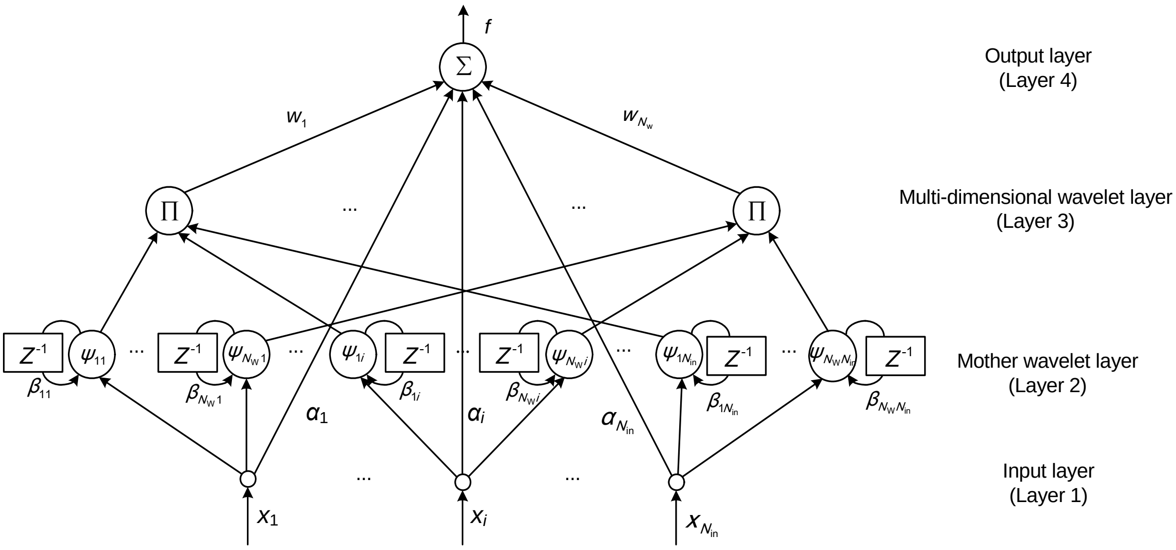

Fig. 2 Structure of the self recurrent wavelet network (SRWN)

In the identification process, we use different methods to update parameters of the SRWN. Parameters in the function ψ (the dilation a_{li}, the translation b_{li} and the self feed-back weight β_{li}) are trained using the gradient descent algorithm to minimize the objective function (Eq. (8)). The updating formula is expressed as

$$\theta(k+1)=\theta(k)-\Gamma\frac{\partial J(k)}{\partial\theta(k)}, \tag{9}$$

where θ represents a_{li}, b_{li} or β_{li}, and Γ is the learning rate. The partial derivatives of $J(k)$ are as follows:

$$\frac{\partial J(k)}{\partial a_{li}}=\sum_{j=1}^{k}\left(\lambda^{k-j}w_l(y(j)-\hat{y}(j))\frac{\chi_{li}(j)}{a_{li}}\cdot\frac{\partial\psi(\chi_{li}(j))}{\partial\chi_{li}(j)}\prod_{m=1,m\neq i}^{N_{in}}\psi\left(\chi_{lm}(j)\right)\right), \tag{10}$$

$$\frac{\partial J(k)}{\partial b_{li}}=\sum_{j=1}^{k}\left(\lambda^{k-j}w_l(y(j)-\hat{y}(j))\frac{1}{a_{li}}\cdot\frac{\partial\psi(\chi_{li}(j))}{\partial\chi_{li}(j)}\prod_{m=1,m\neq i}^{N_{in}}\psi\left(\chi_{lm}(j)\right)\right), \tag{11}$$

$$\frac{\partial J(k)}{\partial \beta_{li}}=-\sum_{j=1}^{k}\left(\lambda^{k-j}w_l(y(j)-\hat{y}(j))\frac{\psi_{li}(j-1)}{a_{li}}\cdot\frac{\partial\psi(\chi_{li}(j))}{\partial\chi_{li}(j)}\prod_{m=1,m\neq i}^{N_{in}}\psi\left(\chi_{lm}(j)\right)\right), \tag{12}$$

where $\chi_{li}(j)=(x_i(j)+\beta_{li}\psi_{li}(j-1)-b_{li})/a_{li}$.

To evolve w_l and α_i on-line, we apply an iterative algorithm, and the derivation is given as follows:

At iteration k, the output of the SRWN is defined as

$$\hat{y}(k)=\sum_{l=1,l\neq l_e}^{N_w}w_l(k-1)\boldsymbol{\psi}_l\left(\boldsymbol{x}(k)\right)+\sum_{i=1,i\neq i_e}^{N_{in}}\alpha_i(k-1)x_i(k)+w_{l_e}\boldsymbol{\psi}_{l_e}\left(\boldsymbol{x}(k)\right)+\alpha_{i_e}x_{i_e}(k), \tag{13}$$

where $\boldsymbol{x}=[x_1, x_2, ..., x_{N_{in}}]^{\mathrm{T}}$, $l_e\in\{1, 2, ..., N_W\}$, $i_e\in\{1, 2, ..., N_{in}\}$, and

$$\boldsymbol{\psi}_l\left(\boldsymbol{x}(k)\right)=\prod_{i=1}^{N_{in}}\psi\left(\frac{x_i(k)+\beta_{li}(k-1)\psi_{li}(k-1)-b_{li}(k-1)}{a_{li}(k-1)}\right). \tag{14}$$

The partial derivative of Eq. (8) with respect to w_{l_e} is

$$\begin{aligned}\frac{\partial J(k)}{\partial w_{l_e}}&=-\sum_{j=1}^{k}\left(y(j)-\hat{y}(j)\right)\boldsymbol{\psi}_{l_e}\left(\boldsymbol{x}(j)\right)\lambda^{k-j}\\&=-\sum_{j=1}^{k}\left[\boldsymbol{\psi}_{l_e}\left(\boldsymbol{x}(j)\right)\lambda^{k-j}\left(y(j)-\sum_{l=1,l\neq l_e}^{N_w}w_l(j-1)\boldsymbol{\psi}_l\left(\boldsymbol{x}(j)\right)-\sum_{i=1,i\neq i_e}^{N_{in}}\alpha_i(j-1)x_i(j)-w_{l_e}\boldsymbol{\psi}_{l_e}\left(\boldsymbol{x}(j)\right)-\alpha_{i_e}x_{i_e}(j)\right)\right].\end{aligned} \tag{15}$$

Let

$$\frac{\partial J(k)}{\partial w_{l_e}} = 0. \tag{16}$$

We can obtain

$$\begin{aligned} w_{l_e} &= \left(\sum_{j=1}^{k} \boldsymbol{\psi}_{l_e}^2 \left(\boldsymbol{x}(j) \right) \lambda^{k-j} \right)^{-1} \\ &\cdot \sum_{j=1}^{k} \left[\left(y(j) - \sum_{l=1, l \neq l_e}^{N_w} w_l(j-1) \boldsymbol{\psi}_l \left(\boldsymbol{x}(j) \right) \right. \right. \\ &\left. \left. - \sum_{i=1, i \neq i_e}^{N_{in}} \alpha_i(j-1) x_i(j) - \alpha_{i_e} x_{i_e}(j) \right) \boldsymbol{\psi}_{l_e} \left(\boldsymbol{x}(j) \right) \lambda^{k-j} \right]. \end{aligned} \tag{17}$$

Define

$$\mathrm{DEN}(k) = \sum_{j=1}^{k} \boldsymbol{\psi}_{l_e}^2 \left(\boldsymbol{x}(j) \right) \lambda^{k-j}, \tag{18}$$

$$\begin{aligned} \mathrm{NUM}(k) &= \sum_{j=1}^{k} \left(y(j) - \sum_{l=1, l \neq l_e}^{N_w} w_l(j-1) \boldsymbol{\psi}_l \left(\boldsymbol{x}(j) \right) \right. \\ &\left. - \sum_{i=1, i \neq i_e}^{N_{in}} \alpha_i(j-1) x_i(j) - \alpha_{i_e} x_{i_e}(j) \right) \boldsymbol{\psi}_{l_e} \left(\boldsymbol{x}(j) \right) \lambda^{k-j}, \end{aligned} \tag{19}$$

$$\begin{aligned} e(k) &= y(k) - \sum_{l=1}^{N_w} w_l(k-1) \boldsymbol{\psi}_l \left(\boldsymbol{x}(k) \right) \\ &- \sum_{i=1, i \neq i_e}^{N_{in}} \alpha_i(k-1) x_i(k) - \alpha_{i_e} x_{i_e}(k). \end{aligned} \tag{20}$$

Hence,

$$\begin{aligned} w_{l_e} &= \frac{\mathrm{NUM}(k)}{\mathrm{DEN}(k)} \\ &= \frac{\lambda \mathrm{NUM}(k-1) + e(k) \boldsymbol{\psi}_{l_e} \left(\boldsymbol{x}(k) \right) + w_{l_e}(k-1) \boldsymbol{\psi}_{l_e}^2 \left(\boldsymbol{x}(k) \right)}{\lambda \mathrm{DEN}(k-1) + \boldsymbol{\psi}_{l_e}^2 \left(\boldsymbol{x}(k) \right)} \\ &= \frac{\mathrm{NUM}(k-1)}{\mathrm{DEN}(k-1)} - \frac{\mathrm{NUM}(k-1)}{\mathrm{DEN}(k-1)} \\ &\quad + \frac{\lambda \mathrm{NUM}(k-1) + e(k) \boldsymbol{\psi}_{l_e} \left(\boldsymbol{x}(k) \right) + w_{l_e}(k-1) \boldsymbol{\psi}_{l_e}^2 \left(\boldsymbol{x}(k) \right)}{\lambda \mathrm{DEN}(k-1) + \boldsymbol{\psi}_{l_e}^2 \left(\boldsymbol{x}(k) \right)} \\ &= w_{l_e}(k-1) + \left(\mathrm{DEN}(k-1) \left(\lambda \mathrm{DEN}(k-1) + \boldsymbol{\psi}_{l_e}^2 \left(\boldsymbol{x}(k) \right) \right) \right)^{-1} \\ &\quad \cdot \left(\lambda \mathrm{NUM}(k-1) \mathrm{DEN}(k-1) + e(k) \mathrm{DEN}(k-1) \boldsymbol{\psi}_{l_e} \left(\boldsymbol{x}(k) \right) \right. \\ &\quad + w_{l_e}(k-1) \mathrm{DEN}(k-1) \boldsymbol{\psi}_{l_e}^2 \left(\boldsymbol{x}(k) \right) \\ &\quad \left. - \lambda \mathrm{DEN}(k-1) \mathrm{NUM}(k-1) - \mathrm{NUM}(k-1) \boldsymbol{\psi}_{l_e}^2 \left(\boldsymbol{x}(k) \right) \right) \\ &= w_{l_e}(k-1) + \frac{e(k) \mathrm{DEN}(k-1) \boldsymbol{\psi}_{l_e} \left(\boldsymbol{x}(k) \right)}{\mathrm{DEN}(k-1) \left(\lambda \mathrm{DEN}(k-1) + \boldsymbol{\psi}_{l_e}^2 \left(\boldsymbol{x}(k) \right) \right)} \\ &= w_{l_e}(k-1) + e(k) \boldsymbol{\psi}_{l_e} \left(\boldsymbol{x}(k) \right) \left(\mathrm{DEN}(k) \right)^{-1}. \end{aligned} \tag{21}$$

When we update w_{l_e}, we take $\alpha_{i_e} = \alpha_{i_e}(k-1)$. Hence, the iterative formulas for w_{l_e} can be written as

$$e(k) = y(k) - \sum_{l=1}^{N_w} w_l(k-1) \boldsymbol{\psi}_l \left(\boldsymbol{x}(k) \right) - \sum_{i=1}^{N_{in}} \alpha_i(k-1) x_i(k), \tag{22}$$

$$\mathrm{DEN}(k) = \lambda \mathrm{DEN}(k-1) + \boldsymbol{\psi}_{l_e}^2 \left(\boldsymbol{x}(k) \right), \tag{23}$$

$$w_{l_e}(k) = w_{l_e}(k-1) + e(k) \boldsymbol{\psi}_{l_e} \left(\boldsymbol{x}(k) \right) \left(\mathrm{DEN}(k) \right)^{-1}. \tag{24}$$

Likewise, the iterative formulas for α_{i_e} can be obtained:

$$e(k) = y(k) - \sum_{l=1}^{N_w} w_l(k-1) \boldsymbol{\psi}_l \left(\boldsymbol{x}(k) \right) - \sum_{i=1}^{N_{in}} \alpha_i(k-1) x_i(k), \tag{25}$$

$$\mathrm{DEN}_\alpha(k) = \lambda \mathrm{DEN}_\alpha(k-1) + x_{i_e}^2(k), \tag{26}$$

$$\alpha_{i_e}(k) = \alpha_{i_e}(k-1) + e(k) x_{i_e}(k) \left(\mathrm{DEN}_\alpha(k) \right)^{-1}. \tag{27}$$

4 Predictive control using SRWN model

The structure of the nonlinear predictive controller based on the SRWN model for the SOFC system is illustrated in Fig. 3. In the control system, the output y is designed to follow the reference output y_r, which is defined as

$$y_r(k+j) = \alpha_r y_r(k+j-1) + (1-\alpha_r) c_r, \tag{28}$$

where c_r is the set point and α_r ($0 \le \alpha_r < 1$) is the parameter that determines the convergence rate of the reference trajectory (Zhu, 2002).

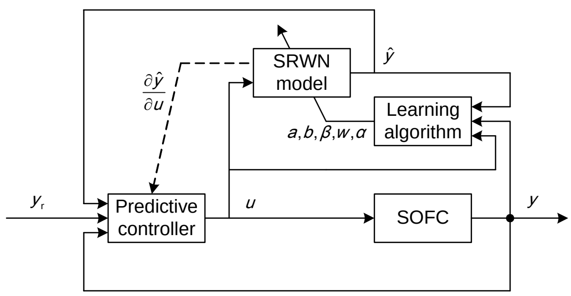

Fig. 3 Structure of the control system using the SRWN model for SOFC

To find an optimum set of inputs, a function over a certain horizon in the future is chosen as the optimality criterion:

$$\varepsilon^{\mathrm{p}}=\frac{1}{2}\sum_{j=N_1}^{N_2}\left(y_{\mathrm{r}}(k+j)-\hat{y}(k+j)\right)^2+\frac{1}{2}\sum_{j=1}^{N_u}\lambda_j^{\mathrm{p}}\left(\Delta u(k+j-1)\right)^2, \quad (29)$$

where N_1 and N_2 are the minimum and maximum costing horizons, respectively, N_u ($\leq N_2$) the control horizon, λ_j^{p} the coefficient, and $\Delta u(k)=u(k)-u(k-1)$. The control signal changes only inside the control horizon and remains constant afterwards (Zhu, 2002). Hence, the control law is determined by minimizing ε^{p}.

Let $\boldsymbol{u}$ be a vector representing the input sequence:

$$\boldsymbol{u}=\left[u(k),u(k+1),\cdots,u(k+N_u-1)\right]^{\mathrm{T}}. \quad (30)$$

The manipulated variable is updated at each iteration using the gradient descent method according to

$$\Delta\boldsymbol{u}=-\mu_{\mathrm{s}}\delta\varepsilon_{\boldsymbol{u}}^{\mathrm{p}}, \quad (31)$$

where μ_{s} is the optimization step, and $\delta\varepsilon_{\boldsymbol{u}}^{\mathrm{p}}$ is the partial derivative of Eq. (29) with respect to $\boldsymbol{u}$.

$$\delta\varepsilon_{\boldsymbol{u}}^{\mathrm{p}}=-\delta\hat{y}_{\boldsymbol{u}}\boldsymbol{e}+\boldsymbol{\lambda}^{\mathrm{p}}\Delta\boldsymbol{u}, \quad (32)$$

where

$$\delta\hat{y}_{\boldsymbol{u}}=\begin{bmatrix}\dfrac{\partial\hat{y}(k+N_1)}{\partial u(k)} & \cdots & \dfrac{\partial\hat{y}(k+N_u)}{\partial u(k)} & \cdots & \dfrac{\partial\hat{y}(k+N_2)}{\partial u(k)}\\ \vdots & & \vdots & & \vdots\\ 0 & \cdots & \dfrac{\partial\hat{y}(k+N_u)}{\partial u(k+N_u-1)} & \cdots & \dfrac{\partial\hat{y}(k+N_2)}{\partial u(k+N_u-1)}\end{bmatrix}, \quad (33)$$

$$\boldsymbol{e}=\left[y_{\mathrm{r}}(k+N_1)-\hat{y}(k+N_1),\cdots,y_{\mathrm{r}}(k+N_2)-\hat{y}(k+N_2)\right]^{\mathrm{T}}, \quad (34)$$

$$\boldsymbol{\lambda}^{\mathrm{p}}=\begin{bmatrix}\lambda_1^{\mathrm{p}} & -\lambda_2^{\mathrm{p}} & 0 & \cdots & 0\\ 0 & \lambda_2^{\mathrm{p}} & -\lambda_3^{\mathrm{p}} & 0 & \vdots\\ \vdots & & & & 0\\ 0 & \cdots & 0 & \lambda_{N_u-1}^{\mathrm{p}} & -\lambda_{N_u}^{\mathrm{p}}\\ 0 & \cdots & \cdots & 0 & \lambda_{N_u}^{\mathrm{p}}\end{bmatrix}. \quad (35)$$

Substituting Eq. (32) into Eq. (31), yields

$$\Delta\boldsymbol{u}=\left(\boldsymbol{I}_{\mathrm{M}}+\mu_{\mathrm{s}}\boldsymbol{\lambda}^{\mathrm{p}}\right)^{-1}\mu_{\mathrm{s}}\delta\hat{y}_{\boldsymbol{u}}\boldsymbol{e}, \quad (36)$$

where $\boldsymbol{I}_{\mathrm{M}}$ is the identity matrix.

Hence, the updating formula for $u(k)$ is given by

$$u(k)=u(k-1)+\left[1,0,\cdots,0\right]\left(\boldsymbol{I}_{\mathrm{M}}+\mu_{\mathrm{s}}\boldsymbol{\lambda}^{\mathrm{p}}\right)^{-1}\mu_{\mathrm{s}}\delta\hat{y}_{\boldsymbol{u}}\boldsymbol{e}. \quad (37)$$

If $0<\mu_{\mathrm{s}}<\dfrac{2}{\lambda_{\max}(\delta\hat{y}_{\boldsymbol{u}}^{\mathrm{T}}\delta\hat{y}_{\boldsymbol{u}})}$ ($\lambda_{\max}(\delta\hat{y}_{\boldsymbol{u}}^{\mathrm{T}}\delta\hat{y}_{\boldsymbol{u}})$ represents the maximum eigenvalue of $\delta\hat{y}_{\boldsymbol{u}}^{\mathrm{T}}\delta\hat{y}_{\boldsymbol{u}}$), the stability of the SRWN-based predictive controller is guaranteed. Using the new measurement, the whole procedure (prediction and optimization) is repeated on-line to find a new input function with the prediction and control horizons moving forward.

The presented controller in this study relies on the SRWN identifiers. Thus, to improve the controller performance, the SRWN model must approximate accurately the outputs of the plant.

5 Simulation results

The operating temperature and fuel utilization are important parameters that have a marked influence on the performance of the SOFC. Hence, we chose the operating temperature and the fuel utilization as model outputs, and the inlet fuel flow rate, inlet air flow rate and current as model inputs. The model of the SOFC can be expressed by the following equations:

$$T(k)=f_1\left(\boldsymbol{M}_{\mathrm{in}}(k-1),\boldsymbol{M}_{\mathrm{in}}(k-2),I(k-1),I(k-2),T(k-1),T(k-2)\right), \quad (38)$$

$$U_{\mathrm{fuel}}(k)=f_2\left(\boldsymbol{M}_{\mathrm{in}}(k-1),\boldsymbol{M}_{\mathrm{in}}(k-2),I(k-1),I(k-2),U_{\mathrm{fuel}}(k-1),U_{\mathrm{fuel}}(k-2)\right), \quad (39)$$

where T is the operating temperature, U_{fuel} the fuel utilization, I the current, and $\boldsymbol{M}_{\mathrm{in}}$ is the vector containing the inlet fuel and air flow rates.

The simulations relate to a planar SOFC stack. The dynamic physical model presented by Li *et al.* (2007) is employed to simulate the real SOFC and to act as the plant in the control system. The operating conditions and parameters of the SOFC are given in Table 1. The SRWN is used for estimating the unknown nonlinear functions (Eqs. (38) and (39)) to approximate the SOFC. The simulations are performed in MATLAB on a computer with a Pentium IV 1.86 GHz CPU and 512 MB RAM.

Table 1 Operating conditions and parameters

Item	Value
Cell area (m^2)	0.18
Number of cells	60
Pressure (Pa)	3×10^5
Electric current (A)	290–360
Stack voltage (V)	35–50
Limiting current density (A/m^2)	9000
Anodic activation energy (J/mol)	1.1×10^5
Cathodic activation energy (J/mol)	1.18×10^5
Inlet fuel flow rate (mol/s)	0.10–0.14
Inlet air flow rate (mol/s)	0.7–2.5
Inlet fuel temperature (K)	1000
Inlet air temperature (K)	1000
Inlet fuel molar composition, CH_4:CO_2:CO:H_2:H_2O	30:1:1:8:60
Inlet air molar composition, O_2:N_2	23:77

The white-box model of the SOFC is excited with the step inputs (inlet fuel flow rate, inlet air flow rate and current) to generate data. The data are split into two parts: one part is used for the identification of the SRWN model and the other for the evaluation. The changing curves of the fuel flow rate, air flow rate and current are shown in Figs. 4–6. Parameters of the SRWN model are initialized as follows:

N_w=26; N_{in}=8; λ=0.9; Γ_a=0.001; Γ_b=0.003; β_{li}=0; a_{li}, DEN(0) and DEN$_\alpha$(0) are given randomly in the range of (0, 1]; b_{li}, w_l and α_i are given randomly in the range of [−1, 1].

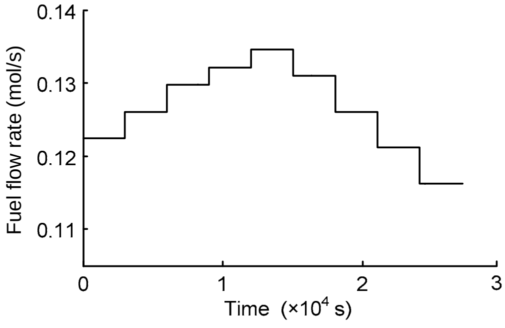

Fig. 4 Inlet fuel flow rate for the evaluation of the SRWN model

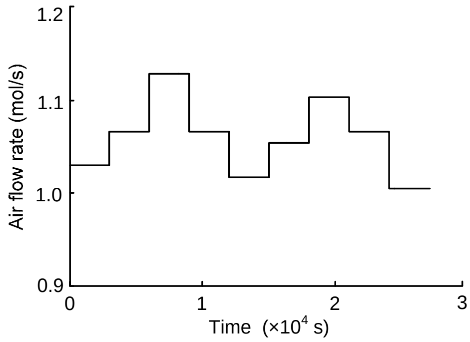

Fig. 5 Inlet air flow rate for the evaluation of the SRWN model

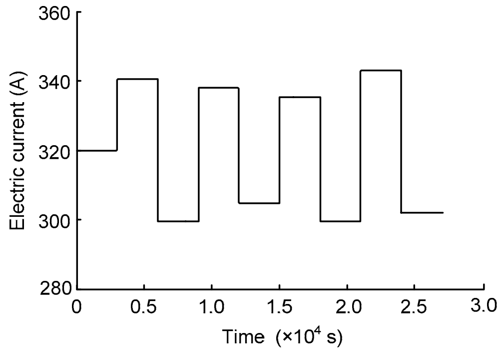

Fig. 6 Current for the evaluation of the SRWN model

Comparisons of the predicted temperature and fuel utilization by the obtained SRWN model with the testing data are shown in Figs. 7 and 8, respectively.

To illustrate the predictive accuracy of the obtained SRWN model, the relative errors ($(\hat{y}-y)/y$) of the predicted and actual values of temperature and fuel utilization are shown in Figs. 9 and 10. Further, the accuracy rating and the root mean squared error (RMSE) are computed using

$$1-\sqrt{\frac{1}{n}\sum_{k=1}^{n}\left(\frac{\hat{y}(k)-y(k)}{y(k)}\right)^2}$$

and

$$\sqrt{\frac{1}{n}\sum_{k=1}^{n}\left(\hat{y}(k)-y(k)\right)^2},$$

respectively. The RMSE and accuracy rating of the predicted temperature are 0.1351 and 0.9998, respectively, while those of the predicted fuel utilization are 0.0004 and 0.9994, respectively. As can be seen from Figs. 7–10 and the statistical results (RMSE and accuracy rating), the predicted results are in good agreement with the actual data.

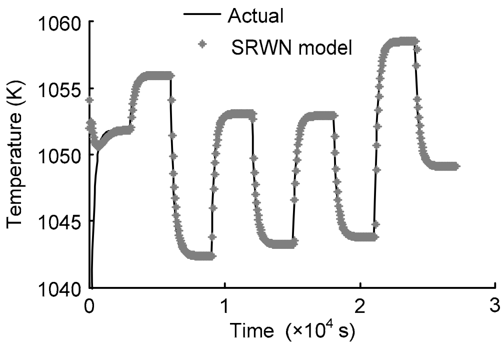

Fig. 7 Temperature predicted by the SRWN model and the actual temperature

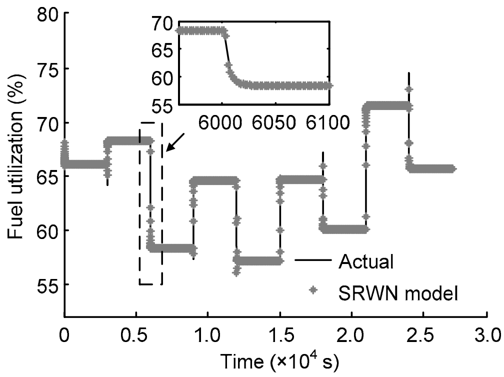

Fig. 8 Fuel utilization predicted by the SRWN model and the actual values

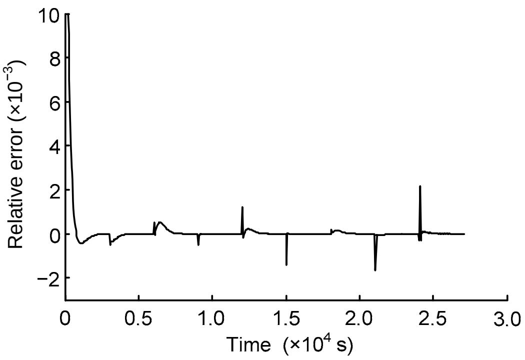

Fig. 9 Relative error of the predicted temperature

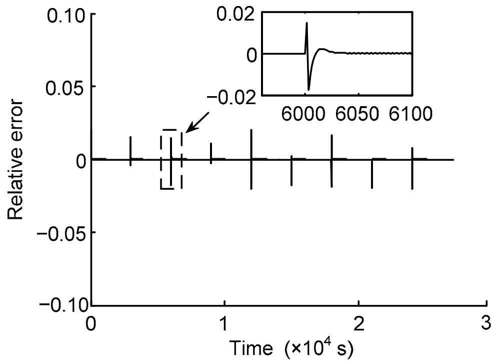

Fig. 10 Relative error of the predicted fuel utilization

Before the predictive control algorithm based on the SRWN model works, the SRWN model is firstly trained off-line. In the process of control, the parameters of the SRWN model can be modified on-line in response to fresh data. Parameters of the controller are given as: N_1=1; N_2=10; N_u=5; α_r=0.2; μ_s=0.05; λ_j^p=0.7 (for normalized data).

The current step changes are taken as disturbances (Fig. 11). The control results of the proposed controller are plotted in Figs. 12–15. To show the advantages of the SRWN-based controller, comparisons of results obtained by the proposed controller and by a traditional fuzzy controller (Schumacher *et al.*, 2004) are also presented (Figs. 12–15).

Because the SRWN model was not trained before predicting the system responses, at the beginning of the identification, the modeling error is significant (Fig. 9). But this error vanishes gradually as the parameters of the SRWN are adjusted. In the subsequent process, several step changes of the operational conditions are set up. These conditions and generated data are fresh to the SRWN model. Owing to the fast convergence of the SRWN, the modeling errors caused by the step changes (new data) vanish rapidly after the sudden increases. The maximum relative error caused by using fresh data is less than 0.002. Hence, to avoid the significant error of the model at the beginning of the identification, off-line training of the SRWN is necessary before the SRWN-based predictive controller works.

The predictive error of the SRWN model might increase at the beginning of the change of the operational conditions, resulting in undesirable actions of the controller. However, the fast learning ability of the SRWN guarantees that the accuracy of the SRWN can be rapidly improved. Therefore, combining with the stability, the SRWN-based controller can rapidly

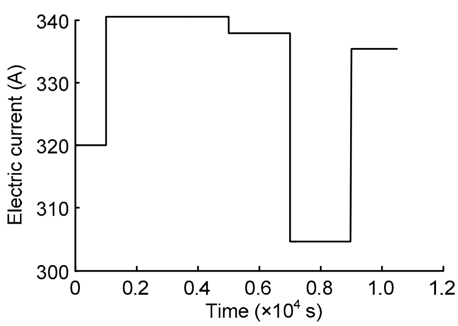

Fig. 11 Step changes of current

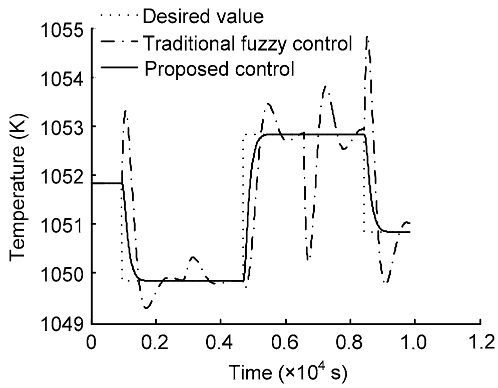

Fig. 12 Temperature control results

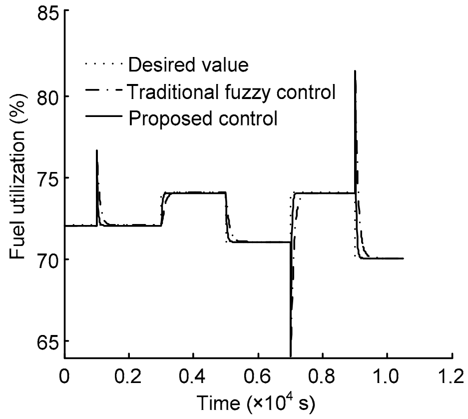

Fig. 13 Results for the control of fuel utilization

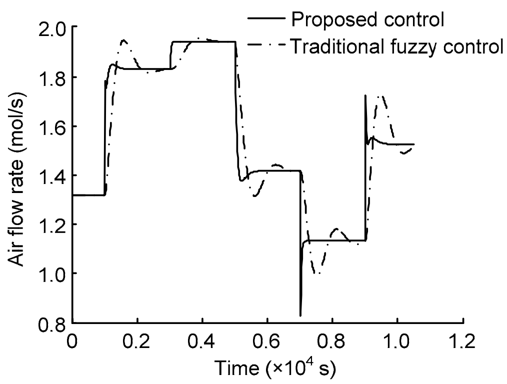

Fig. 14 Manipulated inlet air flow rate

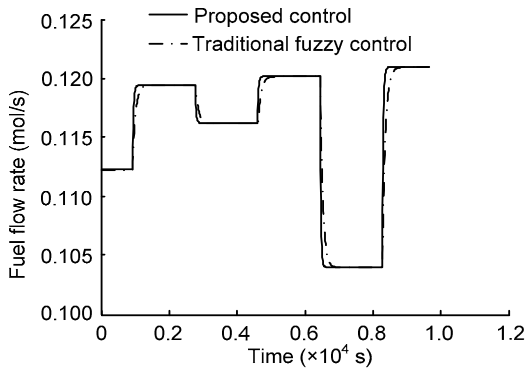

Fig. 15 Manipulated inlet fuel flow rate

adjust the control inputs to compensate for the previous undesirable actions.

It can be seen from the comparisons of control results that there is indeed a performance benefit from using the proposed SRWN-based controller. The responses under the proposed scheme are better than those using the traditional fuzzy controller; faster settling responses of the temperature and fuel utilization with no overshoot are achieved in response to changes of set points and disturbances (temperature, fuel utilization and current).

6 Conclusion

This study presents the application of a nonlinear predictive control system using the SRWN model to control the operating temperature and fuel utilization of a DIR-SOFC. First, the configuration and the operating principles of the DIR-SOFC plant are described. Then, the SRWN is presented in detail to establish the model of the DIR-SOFC, avoiding considering the complex physical and chemical processes in the fuel cells. Based on the SRWN model, the nonlinear predictive controller for the DIR-SOFC is presented. Modeling results show that the SRWN model can predict the dynamic characteristics of the DIR-SOFC with relatively high accuracy. To evaluate the effectiveness of the SRWN-based predictive controller, simulations were carried out using several reference trajectories for different controlled variables (the operating temperature and the fuel utilization). Further, the influence of the load disturbance on the control system was taken into account. Simulation results show that the proposed method is an attractive method for the control of a DIR-SOFC; it has an on-line adapting ability and a fast recovering ability from various disturbances.

References

Arriagada, J., Olausson, P., Selimovic, A., 2002. Artificial neural network simulator for SOFC performance prediction. *Journal of Power Sources*, **112**(1):54-60. [doi:10.1016/S0378-7753(02)00314-2]

Campanari, S., 2001. Thermodynamic model and parametric analysis of a tubular SOFC module. *Journal of Power Sources*, **92**(1-2):26-34. [doi:10.1016/S0378-7753(00)00494-8]

Chan, S.H., Ho, H.K., Tian, Y., 2003. Multi-level modeling of SOFC-gas turbine hybrid system. *International Journal of Hydrogen Energy*, **28**(8):889-900. [doi:10.1016/S0360-3199(02)00160-X]

Chui, C.K., 1992. An Introduction to Wavelets. Academic Press, New York, p.98.

Entchev, E., Yang, L., 2007. Application of adaptive neuro-fuzzy inference system techniques and artificial neural networks to predict solid oxide fuel cell performance in residential microgeneration installation. *Journal of Power Sources*, **170**(1):122-129. [doi:10.1016/j.jpowsour.2007.04.015]

Jurado, F., 2006a. A method for the identification of solid oxide fuel cells using a Hammerstein model. *Journal of Power Sources*, **154**(1):145-152. [doi:10.1016/j.jpowsour.2005.04.005]

Jurado, F., 2006b. Predictive control of solid oxide fuel cells using fuzzy Hammerstein models. *Journal of Power Sources*, **158**(1):245-253. [doi:10.1016/j.jpowsour.2005.08.041]

Karoliussen, H., Nisancioglu, K., Solheim, A., 1998. Use of effective conductivities and unit cell-based supraelements in the numerical simulation of solid oxide fuel cell stacks. *Journal of Applied Electrochemistry*, **28**(3):283-288. [doi:10.1023/A:1003211615845]

Larminie, J., Dicks, A., 2000. Fuel Cell Systems Explained. Wiley, New York, p.164.

Li, J., Cao, G.Y., Zhu, X.J., Tu, H.Y., 2007. Two-dimensional dynamic simulation of a direct internal reforming solid oxide fuel cell. *Journal of Power Sources*, **171**(2):585-600. [doi:10.1016/j.jpowsour.2007.07.029]

Lin, C.H., Wang, C.H., 2006. Adaptive wavelet networks for power-quality detection and discrimination in a power system. *IEEE Transaction on Power Delivery*, **21**(3):1106-1113. [doi:10.1109/TPWRD.2006.874105]

Lin, C.L., Shieh, N.C., Tung, P.C., 2002. Robust wavelet neuro control for linear brushless motors. *IEEE Transaction on Aerospace and Electronic System*, **38**(3):918-932. [doi:10.1109/TAES.2002.1039408]

Oussar, Y., Rivals, I., Personnaz, L., Dreyfus, G., 1998. Training wavelet networks for nonlinear dynamic input-output modeling. *Neurocomputing*, **20**(1-3):173-188. [doi:10.1016/S0925-2312(98)00010-1]

Schumacher, J.O., Gemmar, P., Denne, M., Zedda, M., Stueber, M., 2004. Control of miniature proton exchange membrane fuel cells based on fuzzy logic. *Journal of Power Sources*, **129**(2):143-151. [doi:10.1016/j.jpowsour.2003.10.010]

Selimovic, A., Palsson, J., 2002. Networked solid oxide fuel cell stacks combined with a gas turbine cycle. *Journal of Power Sources*, **106**(1-2):76-82. [doi:10.1016/S0378-7753(01)01051-5]

Shen, C., Cao, G.Y., Zhu, X.J., Sun, X.J., 2002. Nonlinear modeling and adaptive fuzzy control of MCFC stack. *Journal of Process Control*, **12**(8):831-839. [doi:10.1016/S0959-1524(02)00013-6]

Stiller, C., Thorud, B., Seljebo, S., Mathisen, O., Karoliussen, H., Bolland, O., 2005. Finite-volume modeling and hybrid-cycle performance of planar and tubular solid oxide fuel cells. *Journal of Power Sources*, **141**(2):227-240. [doi:10.1016/j.jpowsour.2004.09.019]

Yoo, S.J., Choi, Y.H., Park, J.B., 2006. Generalized predictive control based on self-recurrent wavelet neural network for stable path tracking of mobile robots: adaptive learning rates approach. *IEEE Transaction on Circuits and Systems I*, **53**(6):1381-1394. [doi:10.1109/TCSI.2006.875166]

Zhang, Q., Benveniste, A., 1992. Wavelet networks. *IEEE Transactions on Neural Networks*, **3**(6):889-898. [doi:10.1109/72.165591]

Zhu, J., 2002. Intelligent Predictive Control Technology and Application. Zhejiang University Press, Hangzhou, China, p.36 (in Chinese).